Preferential sliding directions on graphite

S. G. Balakrishna,[1] Astrid S. de Wijn,[2] and Roland Bennewitz[1]

[1]*INM - Leibniz Institute for New Materials and Experimental Physics, Saarland University, Campus D22, 66123 Saarbrücken, Germany*
[2]*Department of Physics, Stockholm University, 10691 Stockholm, Sweden*
(Received 12 April 2014; revised manuscript received 10 June 2014; published 25 June 2014)

The anisotropy of friction on graphitic surfaces is investigated by a combined friction force microscopy and modeling study. Friction vectors deviate up to $15°$ from pulling directions. The strongest deviations are found for pulling directions which lie almost along one zigzag direction of the honeycomb structure, the preferred sliding direction on graphite surfaces and epitaxial graphene grown on SiC(0001). Atomic stick-slip events along and across molecular rows determine direction and magnitude of friction. Simulation and modeling reveal the role of temperature and of the two-dimensional character of the surface potential for the friction anisotropy.

I. INTRODUCTION

Mechanical properties of crystalline materials are ultimately determined by their atomic structure. A direct consequence of the symmetry of the atomic surface structure is anisotropy of friction and wear, the latter of which can be observed on a macroscopic scale [1]. With the introduction of friction force microscopy, atomic-scale friction processes have become experimentally accessible [2].

Anisotropy refers to a dependence of friction on the pulling direction, where both the magnitude of the friction vector and the angular deviation of the friction vector from the direction opposite to the pulling direction may vary. Anisotropy in sliding friction has been observed for several surfaces by means of friction force microscopy [3–13] and also in dynamic atomic force microscopy (AFM) experiments [14,15]. Observations include variations in friction upon rotating the sample [3,4], friction contrast between molecular film domains of different orientation [5,6,14], directional dependence of atomic-scale phenomena [3,15], friction differences between scanning back and forth on a surface with asymmetric molecular orientation [4,7], and deviation of the direction of the friction vector from the pulling direction when scanning in different directions on a crystalline surface [11–13]. These observations have been modeled by various approaches [13,16–19]. Previous studies have focused on the friction in the direction parallel to the sliding motion, as this is the direction of friction generally expected. On anisotropic substrates, however, there is no *a priori* reason why the friction should point in this direction. While some studies [20,21] discuss preferred sliding directions, and some others discuss friction forces perpendicular to the sliding direction [22], these two have not previously been connected in the context of single-asperity friction. There are, however, many examples in the literature of direction locking, when particle motion does not following external driving, but rather some underlying symmetry [23,24]. Without any external driving, directional dependence of diffusivity is also common on rectangular lattices or along step edges. We are interested in preferred sliding directions, by which we mean those high-symmetry directions of the crystalline surface structure which will not show any friction force perpendicular to the pulling direction and which are stable. Slight deviations of the pulling direction from a preferred sliding direction cause strong perpendicular forces which keep the contact sliding along an atomic or molecular row. We emphasize that the anisotropy of the friction on the substrate is a issue different from the dependence of friction on the relative angle of two lattices in a contact, studied for instance in [8,25]; friction anisotropy exists even if the contact area consists of a single atom.

Linear mechanical systems of threefold symmetry (and consequently those of sixfold symmetry) with respect to one axis are isotropic with respect to that axis. In this study we investigate how far the nonlinear nature of friction destroys isotropy on graphitic surfaces, which show sixfold symmetry. In a pioneering work of nanoparticle manipulation by scanning force microscopy, Sheehan and Lieber have shown that nanoparticles slide along preferential directions when pushed on crystalline surfaces with threefold symmetry [20]. Our friction force microscopy, simulation, and modeling study quantifies the anisotropy and provides insight into its atomic mechanisms.

II. EXPERIMENTAL METHODS

Angle-dependent friction measurements were performed on highly oriented graphite surfaces and on graphene layers grown epitaxially on the Si face of 6H-SiC(0001) by the thermal decomposition method in an inert atmosphere [26]. The graphite sample was prepared by exfoliation of the top layers using adhesive tape.

For the experiments we used an Agilent 5500 atomic force microscope (AFM) in ambient conditions. Extra care was taken to mount the cantilever (NANOSENSOR PPP-CONT, nominal stiffness 0.2 N/m) exactly perpendicular to the fast scanning direction at $0°$ scanning angle in the friction mode of the AFM. A small normal force (10–12 nN) was chosen to ensure wearless scanning of the surface, which was confirmed by subsequent imaging. The sample surface was then scanned in all directions in steps of $10°$ or $5°$ without changing the relative orientation of sample and cantilever. The scanning angle was changed between successive scan frames without retracting the tip.

Scanning along directions with a component perpendicular to the cantilever axis will cause a twisting of the cantilever. We will refer to the forces causing the twisting as *x* forces.

Scanning along directions with a component parallel to the cantilever axis will cause buckling of the cantilever. We will refer to the forces causing buckling as y forces. If the z position of the surface is controlled to maintain constant normal force, the apparent change in z position can be used as a linear measure for the y force [10,13]. In our experiments, all scans were recorded at constant height, i.e., with the feedback control for the z position switched off. Average values for frictional x and y forces were calculated by subtracting the average value of forward and backward signals in a cropped scan frame to exclude effects of directional change.

For calibration purposes we also measured the angle-dependent friction response of an isotropic surface, namely an oxidized silicon wafer. These measurements allow one to extract the cantilever-dependent calibration factors for the x and y forces, which must be of equal strength for the isotropic surface [13].

III. SIMULATION METHODS

Sliding friction on graphitic surfaces has been modeled in Refs. [17–20]. Our efforts are based on the Prandtl-Tomlinson model [27–30]. This model is commonly used to describe atomic-scale AFM experiments and has provided understanding of a number of features of atomic friction experiments, such as the stick-slip behavior. The model consists of a support which moves at constant velocity, and which is coupled by a harmonic spring to a tip. The tip is subjected to a substrate potential and viscous damping. The tension in the spring equals the force needed to keep the support moving in the same directions and at constant velocity. The average of this force is the friction force. In our work, we also consider nonzero temperature, and therefore add white noise to the force to create a Langevin thermostat.

For the graphite substrate and the tip with a graphite flake, we use a Prandtl-Tomlinson setup similar to that of Ref. [25]. The substrate consists of a regular arrangement of carbon atoms. The tip is a hexagonal graphite flake of 216 carbon atoms. The interatomic distance within the flake and substrate is 1.42 Å, and the mass of a carbon atom is 1.994423×10^{-26} kg. This system is three-dimensional and both the hexagonal substrate and graphite flake are rigid. The remaining interaction between the carbon atoms is modeled using a realistic potential, namely that of Ref. [31]. The tip is coupled by its center of mass to the support only in the plane of the substrate with a spring constant 1 N/m. A normal load of 108 nN is applied to the flake. The internal degrees of freedom of the flake and substrate are taken into account through the Langevin thermostat with damping parameter 1 ps^{-1}. The flake orientation is kept at the commensurate orientation, as this is the stable orientation of the flake [25]. The support velocity is $v_s = 2$ m/s. While this velocity is much higher than in the experiments, and the load in also higher, these parameters are sufficient for the system to display the same typical stick-slip behavior. The velocities of realistic AFM experiments are typically no more than a μm/s. While there are some computational techniques, such as the parallel replica method [32], which allow one to simulate lower velocities, it is not computationally feasible to reduce the velocity of the simulated system by six orders of magnitude and truly

match the experiments. For an example where such methods are employed to reduce the velocity as much as possible, see Ref. [33].

As an aid to understanding, and because it is analytically more tractible, we also simulate a two-dimensional Prandtl-Tomlinson model with a substrate potential with square symmetry. As this model is not meant to directly represent the physical system, we use dimensionless units. The lattice parameter, tip mass, and potential-energy corrugation are all set to 1. The damping parameter is 5, the spring constant is 5, and the support velocity is 0.0005. As a substrate potential, we use

$$V_{\text{square}}(x,y) = z\left(\tfrac{1}{2} + \tfrac{1}{4}\epsilon_0\right)[\cos(2\pi x) + \cos(2\pi y)]$$
$$+ \tfrac{1}{4}\epsilon_0 \cos(2\pi x)\cos(2\pi y), \qquad (1)$$

with x and y the position coordinates on the substrate, and $\epsilon_0 > -1$. The preferred sliding directions on this lattice are along the x and y axes. The parameter ϵ_0 controls the coupling between the x and y directions. If $\epsilon_0 = 0$, the x and y directions decouple fully. The potential is constructed in such a way that, sliding along a preferred direction following the path of minimum energy, the corrugation experienced by the tip is always the same: unity.

IV. EXPERIMENTAL RESULTS

A. Friction anisotropy on graphite

The results of a friction anisotropy experiment performed on an atomically flat area of highly oriented graphite are summarized in Fig. 1. For a surface with isotropic friction response, end points of the friction vectors should lie on a circle at equal distances. The friction vectors in Fig. 1(a) are concentrated in six groups which form a hexagonal pattern, indicating a strong friction anisotropy. By comparing the directions of friction vector groups with the orientation of the graphite surface which is known from the atomic stick-slip results, we find that the six zigzag directions are preferred sliding directions. A schematic explanation of the experimental result is depicted in Fig. 1(b), visualizing the conclusion of six preferred sliding directions along the zigzag directions of carbon atoms on graphitic surfaces.

In order to understand the experimental results, we have to discuss the case that the pulling direction is not along one of the preferred directions. In this case the friction vector will not have a direction directly opposite to pulling, but rather have an additional component towards the preferred sliding direction. The angular deviation in friction is stronger for pulling directions closer to the preferred directions. In our experimental results, a strong component of the friction force towards the zigzag directions is found for all pulling directions which almost match the zigzag directions, therefore the zigzag directions are preferred sliding directions. One example is the red line in Fig. 1 which points almost along the zigzag direction and shows a strong friction force component towards the zigzag direction. Only when the pulling direction matches exactly one of the preferred sliding directions would the friction vector point in exactly the opposite direction; but this is not the case for any of the 36 pulling directions in Fig. 1. When the pulling direction approaches the armchair direction
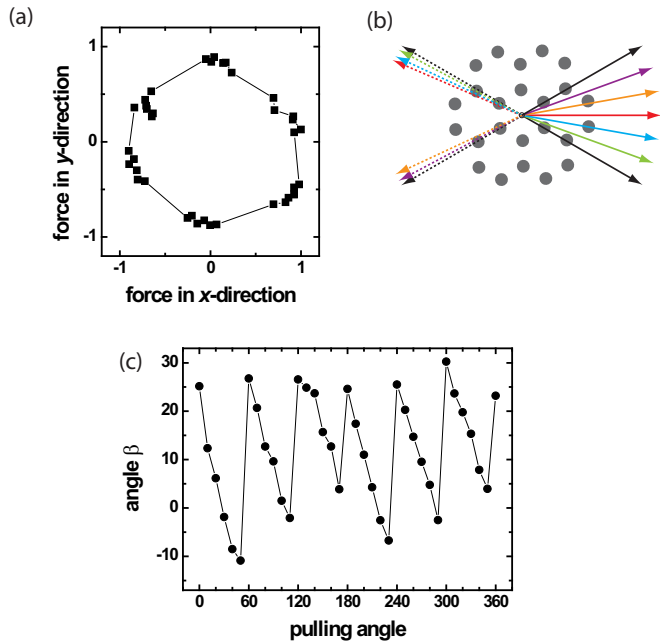
FIG. 1. (Color online) (a) Normalized friction vectors measured for pulling directions between 0° and 360° in steps of 10° on an atomically flat surface area of graphite. The scan size was 27 nm, the scan rate was 3 lines/s. The force values have been scaled to a control experiment on an isotropic silicon oxide surface and normalized with respect to the maximum x force, which was 5.3 nN. (b) Schematic interpretation of the results. Solid arrows indicate the pulling direction, dashed arrows the corresponding direction of the friction force vector. (c) Angle between pulling and friction direction as function of the pulling angle.

[black line in Fig. 1(b)], the angular deviation becomes zero as the armchair direction is exactly in the middle between two preferred sliding directions.

A different representation of the result is given in Fig. 1(c). The angular deviation between friction vector and pulling vector is plotted as a function of the pulling angle. There is a jump at each preferred sliding direction by on average 28.5°. These jumps reflect the strong tendency of the surface to force the contact into the preferred sliding directions. A surprising observation is the strong deviation of the friction vector by about 10–15° for those pulling directions which are only slightly off a zigzag direction. This observation is fully reproduced in our simulations and will be discussed below.

B. Friction anisotropy on graphene/SiC(0001)

The results in Fig. 2 demonstrate that the friction anisotropy due to preferred sliding directions is also found on epitaxial graphene layers grown on a SiC(0001) surface. The surface orientation was different by about 30° as compared to the graphite sample for which results are shown in Fig. 1. Similar to the results in Fig. 1, the endpoints of the friction vectors form six groups in a hexagonal pattern. Two friction vectors, however, lie in the middle between two groups: the ones for 70° and 310° pulling angles. For these two directions, the pulling direction has met almost exactly one of the preferred sliding directions, so that the friction vector is directed opposite to
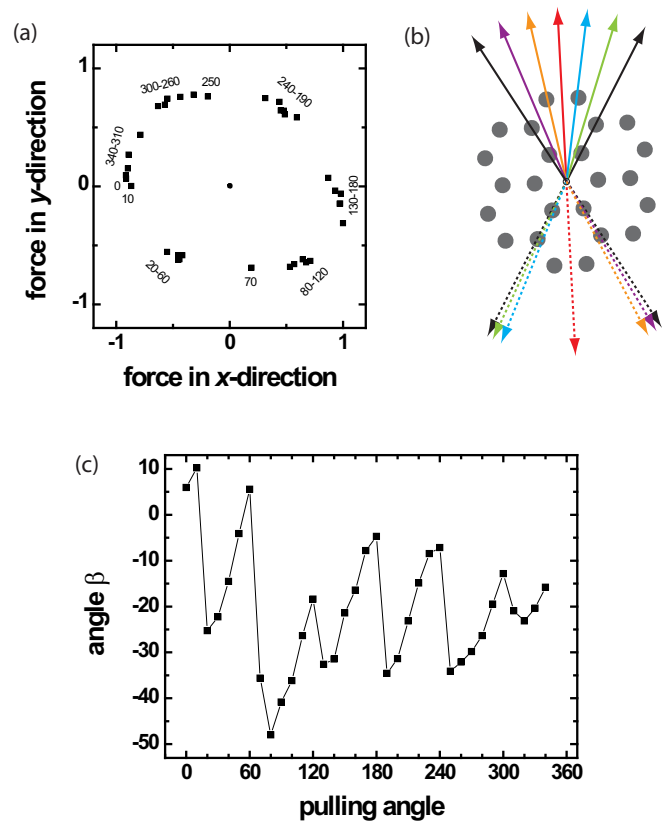
FIG. 2. (Color online) (a) Normalized friction vectors measured for pulling directions between 0° and 340° in steps of 10° on one monolayer of graphene grown epitaxially on a SiC(0001) surface. The scan size was 30 nm, the scan rate 3 lines/s. The labels indicate the pulling direction. The force values have been normalized with respect to the maximum x force, which was 2.0 nN. (b) Schematic interpretation of the results. Solid arrows indicate the pulling direction, dashed arrows the corresponding direction of the friction force vector. (c) Angle between pulling and friction directions as a function of the pulling angle.

the pulling direction. The situation is depicted schematically in Fig. 2(b), where the centered red arrows correspond to the pulling direction of 70° in Fig. 2(a). The plot of the angles between pulling and friction directions in Fig. 2(c) is less regular than the one in Fig. 1(c), but still shows the characteristic jumps at the six preferred sliding directions by about 25°.

The representative force traces in Fig. 3 provide insight into the role of stick-slip instabilities in the anisotropic friction mechanism. Each trace reports x force over the scan range of 30 nm for the different pulling directions. We have already concluded that the pulling angles of 70° and 250° correspond to sliding along a preferred direction, which in this experiment lies almost parallel to the long axis of the cantilever. Therefore, the x-force traces in Fig. 3 give a clear impression of the forces acting perpendicularly to the pulling direction when pulling is close to a preferred direction. There is almost no force fluctuation for the 70° pulling direction. In contrast, there is a pronounced sawtooth signal for the neighboring traces for 60° and 80°, with a characteristic length of 1 to 1.5 nm and opposite sign for 60° and 80° angle. We believe that the sawtooth signal
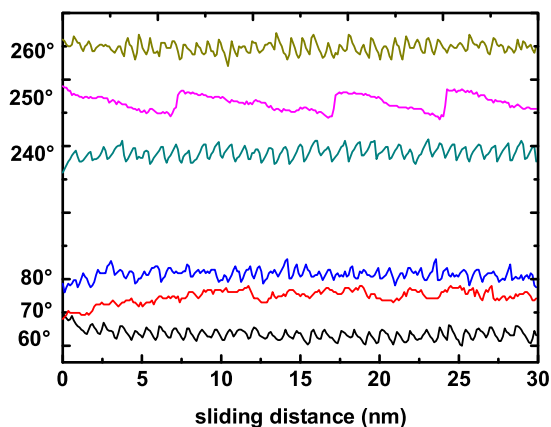
FIG. 3. (Color online) Traces of the force in x direction for pulling directions close to a preferred sliding direction. Since in this configuration the preferred sliding direction is almost parallel to the long axis of the cantilever, forces perpendicular to the pulling direction are measured with high sensitivity as x forces.

indicates atomic slips of the contact from one atomic row to the next atomic row due to the $10°$ misalignment between the preferred zigzag direction and the pulling direction. The contact slides along the atomic rows of the zigzag direction, until the increasing perpendicular force initiates a slip to the adjacent row. The distance between adjacent rows of hexagonal patterns is $\sqrt{3}/2 \times 0.246\,\mathrm{nm} = 0.213\,\mathrm{nm}$, therefore we expect a slip every $0.213\,\mathrm{nm}/\tan(10°) = 1.21\,\mathrm{nm}$ in agreement with the experimental observations. A very similar observation is made for the opposite pulling direction at an angle of $250°$. In this case, the zigzag direction is not perfectly matched, as indicated by slips to the adjacent row every 5 nm. The misalignment can be calculated to be $2.4°$.

Friction anisotropy on epitaxial graphene on SiC(0001) for a smaller scan range and a finer resolution in pulling angles is reported in Fig. 4. The overall shape of the curve is similar to Fig. 2. There is some distortion in the curve probably due to a gradual change in the tip-sample contact area over the course of this long experiment. Friction vectors predominantly point
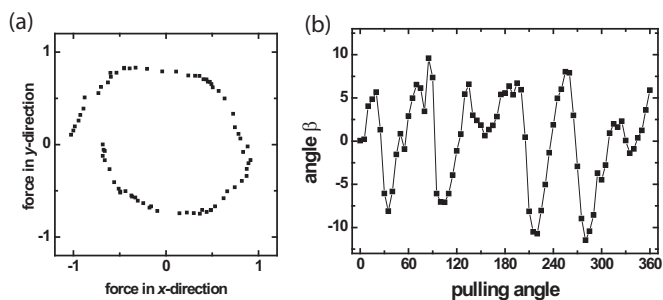
FIG. 4. (a) Normalized friction vectors measured for pulling directions between $0°$ and $360°$ in steps of $5°$ on one monolayer of graphene grown epitaxially on a SiC(0001) surface. The scan size was 5 nm, the scan rate 12 lines/s. Friction has increased over the course of this long experiment, probably due an increase in contact area. The force values have been normalized with respect to the maximum x force, which was 4.4 nN. (b) Angle between pulling and friction directions as a function of the pulling angle.
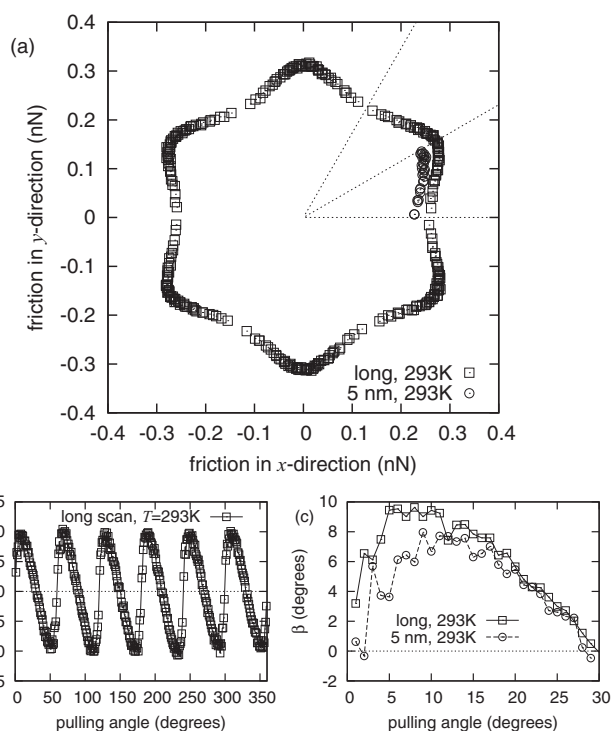
FIG. 5. Friction anisotropy in simulations of a 216-atom graphite flake at room temperature. (a) Friction vector plot with steps of $1°$; (b) and (c) the angle between the friction force and the pulling directions. The relative angle between friction and sliding β is antisymmetric around vanishing sliding angle, so that there is a rapid change from positive to negative β around the origin in (c) and in Fig. 7(b). The dotted lines in the friction vector plot are at $0°$, $30°$, and $60°$ and are included as a guide to the eye.

in six directions, confirming again the zigzag directions of the graphene surface structure as preferred sliding directions. For this smaller scan range, the angular concentration is less pronounced. The overall shape of the curve is not circular but hexagonal. The absolute friction values are higher in armchair directions as compared to zigzag directions. The plot of the angle between friction and pulling directions is somewhat distorted, but still shows the sixfold symmetry and a softer transition by about $15°$ around the preferred sliding directions.

V. MODELING RESULTS

Results of simulations of the anisotropy in the friction of the 216-atom flake at room temperature are shown in Fig. 5. The hexagonal symmetry of the lattice is preserved in the friction vector plot [Fig. 5(a)]. The friction is largest in the armchair directions. The zigzag directions, which are the preferred sliding directions, have smaller friction. As in the experiments, when the pulling direction deviates from one of the symmetry axes of the lattice, the friction does not point directly opposite to the sliding, but there is an extra component perpendicular to the pulling direction that pulls the sliding towards a preferred sliding direction. This can be seen in Figs 5(b) and 5(c).

Force traces are shown in Fig. 6. For pulling directions close to the preferred sliding directions, there are distinctive slips seen in the perpendicular direction with a long distance
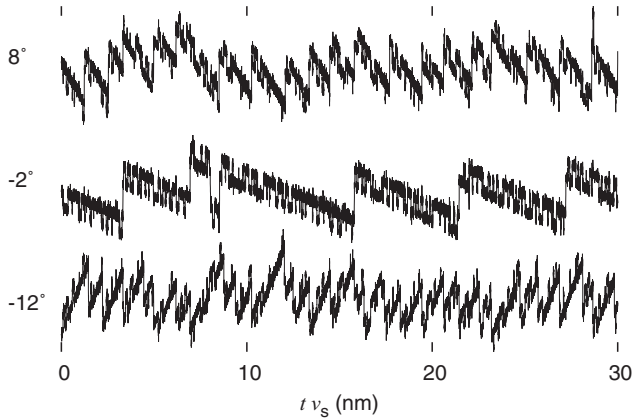
FIG. 6. Friction anisotropy in simulations of a 216-atom graphite flake at room temperature: forces in the direction perpendicular to the preferred sliding direction for various sliding angles. This plot should be compared to Fig. 3.

FIG. 7. Friction anisotropy in simulations of a 216-atom graphite flake at various temperatures: (a) upper right quadrant of the friction vector plot with steps of 1° and (b) relative angle between friction and sliding for a few different temperatures.

traveled in between, shown in the bottom line in Fig. 6. Such behavior was noted in Ref. [34], and was attributed there to puckering of the top layer of the substrate. Since the simulated substrate in this work is rigid, puckering is impossible, and cannot be the origin of the long slips with long sticks in between. These long slips can be understood when one considers slipping along the preferred direction and perpendicular to it. When the pulling direction is close to a preferred direction, the support travels very slowly in the direction perpendicular to the preferred direction. Slips therefore occur in this direction after a longer distance has been traveled along the preferred sliding direction.

For comparison, we have simulated also sliding over a short distance. In this case, as can be seen from Fig. 5(c), there is no strong transverse component of friction close to the preferred sliding direction, due to the fact that, over the short distance, no slip occurs at all in the transverse direction. Averaging over back and forth trajectories then leads to a vanishing transverse component. The parallel friction force is also somewhat smaller, as the initial buildup before the first slip contributes significantly. It should be noted that, in order to eliminate the significant noise due thermal fluctuations on the results for these short scans, we actually average over 20 simulated trajectories. When we simulated long scans, we always started the averaging after the first slip in the transverse direction. We also made sure that the support traveled an integer number of lattice periods in the direction perpendicular to the preferred sliding direction. This means that our simulation results are equivalent to infinite scans, apart from the effects of thermal fluctuations.

From Fig. 7, one can see that the anisotropy changes with temperature. In particular, the jump in angle when the pulling direction passes through a preferred direction is higher at low temperatures. Below, we explain the qualitative behavior of the anisotropy on the hexagonal lattice by focusing on a similar system that is easier to understand analytically, namely a square lattice.

First, we consider the case with $\epsilon_0 = 0$ [see Eq. (1)], when the dynamics in the x and y directions decouple completely. This does not imply that the dynamics or the
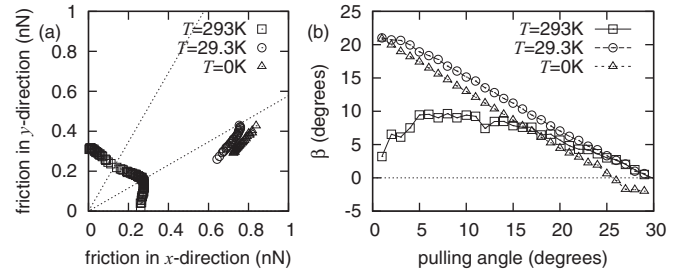
friction become isotropic. Both components simply behave as a one-dimensional Prandtl-Tomlinson model with two different sliding velocities. If the friction is independent of the sliding velocity, which is the case for sufficiently slow sliding at temperature equal to zero, the x and y components of the friction are thus always equal to each other. In this case, the friction always points in one of the four directions precisely in between the preferred sliding directions. The friction vector plot consists only of four points, and $\beta(\phi) = \pi/4 - \phi$ if $\phi \in \langle 0, \pi/2 \rangle$. This can also be seen in the simulation results for $\epsilon_0 = 0$, $T = 0$ shown in Fig. 8.

When the temperature is nonzero, a velocity dependence of the friction is introduced. For slow sliding velocities, the friction is reduced [35,36]. This is due to the thermal activation of slips. In the two-dimensional Prandtl-Tomlinson model, the component of the velocity perpendicular to a preferred sliding direction is small if the pulling direction deviates only slightly from the preferred direction. Thus, at finite temperature, the perpendicular component of the friction in this case becomes small and the anisotropy is reduced. This can be seen in Figs. 8(a) and 8(c) where β is typically smaller for higher temperature.

As analytical results for the temperature and velocity dependence of friction in the Prandtl-Tomlinson model exist [35], we can be more specific. At low temperatures, and low but not extremely low sliding velocities, the temperature and velocity dependence can be written as

$$F_{\mathrm{fric}}(v,T) = F_0 - \left| \frac{T}{l_0} \right|^{\frac{2}{3}} \left| \ln \frac{v}{f_0 T} \right|^{\frac{2}{3}}, \qquad (2)$$

where F_0 is the friction force for zero temperature, T is the temperature in energy units, v is the sliding velocity, and l_0 and f_0 are constants. We now need to compare the two components with different velocities $v_s \cos\phi$ and $v_s \sin\phi$, where ϕ is the sliding direction. Thus, we find that

$$F_x(\phi) = F_0 + c_1 T^{\frac{2}{3}} | \ln\cos\phi - \ln T + c_2 |^{\frac{2}{3}}, \qquad (3)$$

$$F_y(\phi) = F_0 + c_1 T^{\frac{2}{3}} | \ln\sin\phi - \ln T + c_2 |^{\frac{2}{3}}, \qquad (4)$$

$$\beta(\phi) = \arctan \frac{F_y(\phi)}{F_x(\phi)} - \phi, \qquad (5)$$
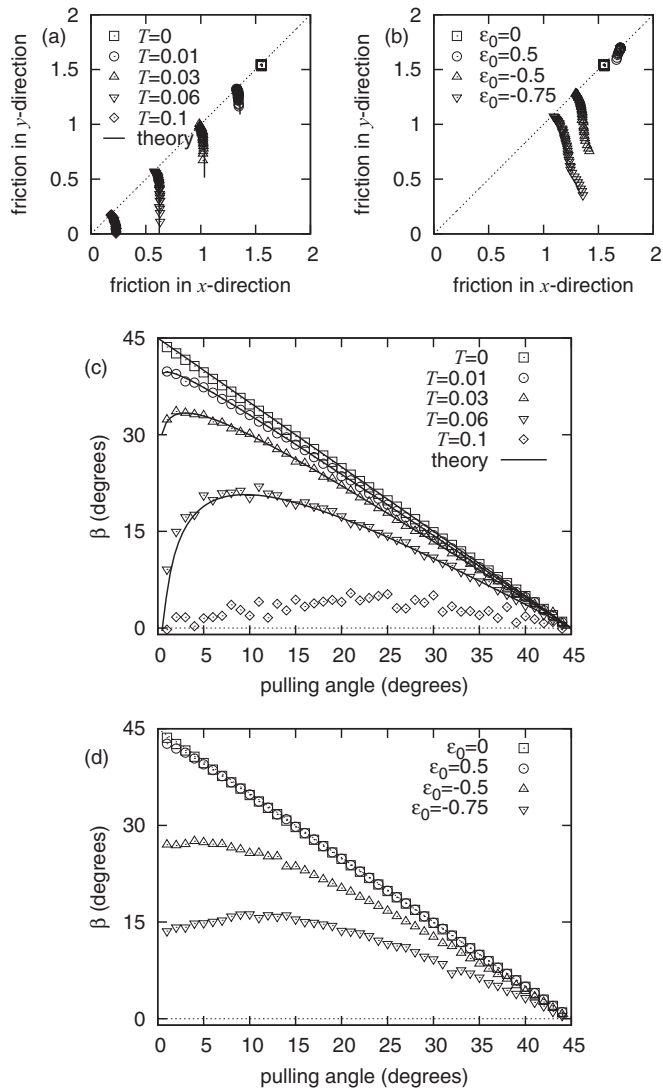
FIG. 8. A parameter study of friction anisotropy on square lattices. Points represent simulation results and solid lines are based on the theoretical dependence on velocity and temperature. Subfigures (a) and (c) show the dependence of anisotropy on temperature, while (b) and (d) show the effects of coupling between the x and y directions. The friction vector plots are shown with steps of $1°$. The dotted lines are included as a guide to the eye. The relative angle between friction and pulling β is antisymmetric around vanishing pulling angle, so that there is a rapid change from positive to nagive β around the origin in (c) and (d).

with c_1 and c_2 constants. By fitting to the simulation results, while taking into account the conditions under which Eq. (2) is valid, we find that $c_1 \approx -2.4$, $c_2 \approx -6.8$, $F_0 \approx 1.55$. The fitted lines are shown alongside the simulation results in Figs. 8(a) and 8(c). For $T = 0.1$ times the corrugation, Eq. (2) is no longer sufficiently accurate. For any finite temperature, there is no jump in the angle of friction close to the sliding angle, but rather a rapid change.

In substrates with hexagonal symmetry such as graphite, where there are three instead of two preferred sliding directions, dynamics along the different preferred sliding directions cannot decouple. We therefore also investigate the effect of such coupling in the square lattice. We use the parameter ϵ_0 in

Eq. (1) to control the coupling between the x and y directions. Results of simulations for various values of ϵ_0 are shown in Figs. 8(b) and 8(d). For $\epsilon_0 > 0$, friction is higher and remains strongly anisotropic. When $\epsilon_0 < 0$, friction becomes lower, and more isotropic.

This can be explained when one considers how the tip sticks and slips, and what kind of forces must be overcome for the tip to slip. In the Prandtl-Tomlinson model at constant pulling velocity, if the tip slips later, there is more time for tension to build up in the spring, and friction is generally higher. We note that the force to be overcome in order to slip is closely related to the energy barrier that the tip travels over during the slip. Below, we use the two concepts interchangeably.

We first consider the case of $\epsilon_0 > 0$. In this case more force is required for the tip to slip than for $\epsilon = 0$ whenever the tip is away from a potential minimum in the other direction. As a result, slips in one preferred sliding direction occur whenever the tip is close to the minimum in the other direction. When the pulling direction is close to a preferred direction, this means that the perpendicular component has many opportunities to slip and the friction in this direction is approximately the same as it is for $\epsilon_0 = 0$. Along the preferred direction, however, the tip will have to overcome higher energy barriers and forces. Consequently, the tip slips later and friction increases. In Fig. 8(b), the points for $\epsilon_0 = 0.5$ with the lowest friction in the y direction correspond to angles close to 0 degrees. When the pulling direction deviates from a preferred direction, the tip has fewer optimal opportunities to slip in either direction, and both components of the friction increase. This can also be seen in the figure.

When $\epsilon_0 < 0$, the opposite happens. Less force is needed to slip in the perpendicular direction when the tip is not in a potential minimum. When the tip travels along a direction close to a preferred sliding direction, this means that the forces (energy barriers) that must be overcome in the perpendicular direction actually decrease. The component of the friction force perpendicular to the preferred sliding direction is therefore also lower than for $\epsilon = 0$. The component parallel to the preferred sliding direction also decreases, but not by as much, because in this direction, the tip must sometimes still overcome the original barrier of unity when it is traveling through potential minima. The result is that the anisotropy also decreases. This can be seen clearly in Figs. 8(b) and 8(d). However, unlike in the case of thermal noise, the coupling does not remove the angular discontinuity at the preferred sliding directions.

VI. DISCUSSION

Our experimental results reveal a strong anisotropy of single-asperity friction on graphitic surfaces. The zigzag directions of the honeycomb structure are preferred sliding directions. Pulling into a direction which deviates slightly from a zigzag direction produces a significant perpendicular component of the friction vector which keeps the contact sliding along the zigzag direction. As a result, the angle between pulling direction and resulting friction vector jumps by up to 30 degrees. Atomic-scale experiments reveal that the perpendicular component of the friction vector exhibits stick-slip dynamics. The perpendicular force increases while the tip is sliding along the zigzag direction until it is strong

enough to initiate a slip of the contact into the adjacent zigzag row. Highly oriented graphite surfaces and graphene layers grown epitaxially on SiC(0001) show similar results. The degree of anisotropy as expressed in the jump of the angle between pulling and friction decreases for very small scan ranges. Friction vectors antiparallel to the pulling direction are found only when the pulling direction matches exactly a zigzag direction or if it matches one of the armchair directions. Therefore, experimental series with equiangular pulling directions result in a clustering of the friction vectors around the armchair directions. Experiments with higher angular resolution on smaller scan ranges indicate that the absolute value of the friction vectors is maximal in armchair directions and minimal in the preferred zigzag directions. The increasing probability of a sudden change in the structure of the tip apex limits the duration and possible resolution of the experiments.

We have no means to determine the atomic structure of the tip apex sliding on the graphitic surfaces. While experimental indications for the transfer of graphene flakes in friction experiments have been discussed before [37], direct observation of the process has only been possible *in situ* transmission electron microscopy experiments [38]. Qualitatively the results on friction anisotropy do not depend on whether the tip is amorphous silicon oxide, carries a flake of graphene, or has some other semi-crystalline structure. For a nanometer-scale contact, contributions to the force from the finite number of atoms at the tip apex will reveal the symmetry of the crystalline substrate regardless of the precise structure of the contact [21]. The structure of the contact appears only in the scaling of the friction with contact area [39]. Throughout all experiments, we have observed atomic-scale stick-slip with the expected hexagonal periodicity of graphene, leading us to the conclusion that our tip was amorphous silicon oxide or a graphene flake, the latter not rotated but in orientational registry with the substrate [37,40].

The simulation results for graphite flakes on graphite reproduce the experiments well. A similar star shape is observed with preferred sliding directions along the armchair direction. Away from the preferred sliding directions, the component of the friction force perpendicular to the pulling direction increases rapidly. At lower temperature, this happens more abruptly. It should be noted that the precise parameters of the experiments are not reproduced in the simulations. The extremely low velocities of AFM experiments cannot be achieved in molecular-dynamics simulations. As the nature of the contact (crystalline graphene flake or amorphous silicon oxide) and its size is unknown, the corrugation that the tip experiences cannot be estimated. In addition, the force field for carbon does, as do many similar force fields, underestimate the corrugation of a carbon atom on the surface [41]. A silicon oxide tip apex is likely to have an even higher corrugation than a graphite flake. Nevertheless, qualitatively, the simulation results are not far away from the experiments. This is due to the fact that, in the Tomlinson model, the sliding velocity affects the friction only in the temperature dependence, and then only logarithmically [see Eq. (2)]. Furthermore, underestimation of the corrugation increases the effects of temperature and compensates for the difference in sliding velocity.

While the model used in this work is relatively simple, including additional effects would not yield a qualitatively different result. The energy landscape experienced by the tip must always follow the same periodicity as the substrate. Effects such as distortion of the flake edges, which can significantly alter some aspects of friction [42], flake reorientation, and tip structure cannot change this. Translational symmetry, however, only relates to rotational symmetry if the tip has the same rotational symmetry as the substrate. A circular amorphous tip has no inherent anisotropy. Thus, a sufficiently large amorphous silicon oxide tip apex instead of a crystalline flake fixed to the tip, as we have modeled the contact here, would not lead to qualitatively different results. Any additional anisotropy of the tip itself can still play a role. A highly asymmetric tip, or a tip with different rotational symmetry than the substrate, might produce some additional anisotropy in the friction. Nevertheless, the anisotropy of the substrate lattice is always present in the friction anisotropy. In a full description which included the internal degrees of freedom of the tip and substrate, these can act as a heat bath, absorbing kinetic energy of the tip center of mass. This could be modeled simply as a higher effective damping parameter in the Prandtl-Tomlinson model, possibly with a spatial dependence with the same periodicity and symmetry as the substrate. Because the regime under study here is close to quasistatic, it is the energy landscape of the interaction between the tip and substrate that dominates the diffusion, and such additional damping would also not change the results.

The simulations of the two-dimensional Tomlinson model with a square potential give further insight into the origins of the effects seen in the experiments as well as the graphitic simulations. The friction anisotropy is the most extreme at low temperature and when the x and y directions do not couple. At zero temperature, there is a discontinuous jump in the transverse component of the friction force around the preferred sliding direction. For finite temperature, this jump becomes a rapid change. We conclude that the shape of the friction vector plot is actually an interplay between different effects of temperature and substrate geometry. Nevertheless, the symmetries of the friction vector plot are determined by the substrate lattice and the preferred sliding directions.

In summary, the nonlinear mechanisms described above result in anisotropic friction on graphitic surfaces despite their sixfold symmetry. An important observation is the strongest deviation in direction of the friction vector from the pulling direction when pulling almost along a preferential sliding direction. The observation explains the strong directional preference in nanoparticle manipulation. Simulations provide unique insights into the role of temperature and of the two-dimensional character of the surface potential. Increasing temperature softens the effects of anisotropy through the velocity dependence of different friction components at higher temperatures.

[1] Y. Enomoto and D. Tabor, Proc. R. Soc. London Ser. A **373**, 405 (1981).

[2] C. M. Mate, G. M. McClelland, R. Erlandsson, and S. Chiang, Phys. Rev. Lett. **59**, 1942 (1987).

[3] R. M. Overney, H. Takano, M. Fujihira, W. Paulus, and H. Ringsdorf, Phys. Rev. Lett. **72**, 3546 (1994).

[4] H. Bluhm, U. D. Schwarz, and K. P. Meyer, Appl. Phys. A **61**, 525 (1995).

[5] M. Liley, D. Gourdon, D. Stamou, U. Meseth, T. M. Fischer, C. Lautz, H. Stahlberg, H. Vogel, N. A. Burnham, and C. Duschl, Science **280**, 273 (1998).

[6] R. W. Carpick, D. Y. Sasaki, and A. R. Burns, Tribology Lett. **7**, 79 (1999).

[7] H. Shindo, K. Shitagami, T. Sugai, and S.-i. Kondo, Phys. Chem. Chem. Phys. **1**, 1597 (1999).

[8] M. Dienwiebel, G. S. Verhoeven, N. Pradeep, J. W. M. Frenken, J. A. Heimberg, and H. W. Zandbergen, Phys. Rev. Lett. **92**, 126101 (2004).

[9] M. Kwak and H. Shindo, Phys. Chem. Chem. Phys. **6**, 129 (2004).

[10] J. Y. Park, D. F. Ogletree, M. Salmeron, R. A. Ribeiro, P. C. Canfield, C. J. Jenks, and P. A. Thiel, Science **309**, 1354 (2005).

[11] V. Kalihari, G. Haugstad, and C. D. Frisbie, Phys. Rev. Lett. **104**, 086102 (2010).

[12] M. Campione and E. Fumagalli, Phys. Rev. Lett. **105**, 166103 (2010).

[13] M. Campione, S. Trabattoni, and M. Moret, Tribology Lett. **45**, 219 (2012).

[14] M. S. Marcus, R. W. Carpick, D. Y. Sasaki, and M. A. Eriksson, Phys. Rev. Lett. **88**, 226103 (2002).

[15] A. J. Weymouth, D. Meuer, P. Mutombo, T. Wutscher, M. Ondracek, P. Jelinek, and F. J. Giessibl, Phys. Rev. Lett. **111**, 126103 (2013).

[16] J. A. Harrison, C. T. White, R. J. Colton, and D. W. Brenner, Phys. Rev. B **46**, 9700 (1992).

[17] P. Steiner, R. Roth, E. Gnecco, A. Baratoff, and E. Meyer, Phys. Rev. B **82**, 205417 (2010).

[18] E. Gnecco, O. Y. Fajardo, C. M. Pina, and J. J. Mazo, Tribology Lett. **48**, 33 (2012).

[19] G. S. Verhoeven, M. Dienwiebel, and J. W. M. Frenken, Phys. Rev. B **70**, 165418 (2004).

[20] P. E. Sheehan and C. M. Lieber, Science **272**, 1158 (1996).

[21] A. S. de Wijn, Phys. Rev. B **86**, 085429 (2012).

[22] N. Sasaki, K. Kobayashi, and M. Tsukada, Phys. Rev. B **54**, 2138 (1996).

[23] P. T. Korda, M. B. Taylor, and D. G. Grier, Phys. Rev. Lett. **89**, 128301 (2002).

[24] D. Speer, R. Eichhorn, and P. Reimann, Phys. Rev. Lett. **102**, 124101 (2009).

[25] A. S. de Wijn, C. Fusco, and A. Fasolino, Phys. Rev. E **81**, 046105 (2010).

[26] K. V. Emtsev, A. Bostwick, K. Horn, J. Jobst, G. L. Kellogg, L. Ley, J. L. McChesney, T. Ohta, S. A. Reshanov, J. Rohrl *et al.*, Nat. Mater. **8**, 203 (2009).

[27] G. A. Tomlinson, Philos. Mag. **7**, 905 (1929).

[28] L. Prandtl, Z. Angew. Math. Mech. **8**, 6 (1928).

[29] V. L. Popov and J. A. T. Gray, Z. Angew. Math. Mech. **92**, 683 (2012).

[30] M. H. Müser, Phys. Rev. B **84**, 125419 (2011).

[31] J. H. Los and A. Fasolino, Phys. Rev. B **68**, 024107 (2003).

[32] B. P. Uberuaga, S. J. Stuart, and A. F. Voter, Phys. Rev. B **75**, 014301 (2007).

[33] Q. Li, Y. Dong, D. Perez, A. Martini, and R. W. Carpick, Phys. Rev. Lett. **106**, 126101 (2011).

[34] M. V. Rastei, B. Heinrich, and J. L. Gallani, Phys. Rev. Lett. **111**, 084301 (2013).

[35] Y. Sang, M. Dubé, and M. Grant, Phys. Rev. Lett. **87**, 174301 (2001).

[36] K. B. Jinesh, S. Y. Krylov, H. Valk, M. Dienwiebel, and J. W. M. Frenken, Phys. Rev. B **78**, 155440 (2008).

[37] M. Dienwiebel, N. Pradeep, G. Verhoeven, H. Zandbergen, and J. Frenken, Surf. Sci. **576**, 197 (2005).

[38] A. P. Merkle and L. D. Marks, Appl. Phys. Lett. **90**, 064101 (2007).

[39] M. H. Mueser, Europhys. Lett. **66**, 97 (2004).

[40] A. E. Filippov, M. Dienwiebel, J. W. M. Frenken, J. Klafter, and M. Urbakh, Phys. Rev. Lett. **100**, 046102 (2008).

[41] M. Reguzzoni, A. Fasolino, E. Molinari, and M. C. Righi, Phys. Rev. B **86**, 245434 (2012).

[42] M. M. van Wijk, M. Dienwiebel, J. W. M. Frenken, and A. Fasolino, Phys. Rev. B **88**, 235423 (2013).